Impacts of the North Atlantic Warming Hole in Future Climate Projections: Mean Atmospheric Circulation and the North Atlantic Jet®

MELISSA GERVAIS

Department of Meteorology and Atmospheric Science, and The Institute for CyberScience, The Pennsylvania State University, University Park, Pennsylvania, and Lamont–Doherty Earth Observatory, Columbia University, New York, New York

JEFFREY SHAMAN

Department of Environmental Health Sciences, Columbia University, New York, New York

YOCHANAN KUSHNIR

Lamont-Doherty Earth Observatory, Columbia University, New York, New York

(Manuscript received 28 September 2018, in final form 25 January 2019)

ABSTRACT

In future climate simulations there is a pronounced region of reduced warming in the subpolar gyre of the North Atlantic Ocean known as the North Atlantic warming hole (NAWH). This study investigates the impact of the North Atlantic warming hole on atmospheric circulation and midlatitude jets within the Community Earth System Model (CESM). A series of large-ensemble atmospheric model experiments with prescribed sea surface temperature (SST) and sea ice are conducted, in which the warming hole is either filled or deepened. Two mechanisms through which the NAWH impacts the atmosphere are identified: a linear response characterized by a shallow atmospheric cooling and increase in sea level pressure shifted slightly downstream of the SST changes, and a transient eddy forced response whereby the enhanced SST gradient produced by the NAWH leads to increased transient eddy activity that propagates vertically and enhances the midlatitude jet. The relative contributions of these two mechanisms and the details of the response are strongly dependent on the season, time period, and warming hole strength. Our results indicate that the NAWH plays an important role in midlatitude atmospheric circulation changes in CESM future climate simulations.

1. Introduction

Sea surface temperatures (SSTs) are projected to increase in most of the world's oceans as a result of global climate change. However, within the North Atlantic subpolar gyre south of Greenland, there is a striking deficit in warming in global climate model projections that is commonly referred to as the North Atlantic warming hole (NAWH) (Drijfhout et al. 2012; Rahmstorf et al. 2015; Gervais et al. 2018; Woollings et al. 2012; Marshall et al. 2015). There is some evidence of reduced warming in the NAWH region in observations

© Supplemental information related to this paper is available at the Journals Online website: https://doi.org/10.1175/JCLI-D-18-0647.s1.

Corresponding author: Melissa Gervais, mmg62@psu.edu

(Rahmstorf et al. 2015; Drijfhout et al. 2012); furthermore, this deficit in warming relative to global average SST increase is predicted to become greater and more apparent relative to the internal ocean variability as the twenty-first century progresses (Gervais et al. 2018). These changes in SST pattern occur as the result of changes in ocean circulation (Gervais et al. 2018; Winton et al. 2013; Woollings et al. 2012) and could have a significant impact on atmospheric circulation (Gervais et al. 2016) and the North Atlantic storm track (Woollings et al. 2012) in the future. Understanding the potential impact of the NAWH on atmospheric circulation and the responsible mechanisms is the focus of the current study.

Previous studies have related NAWH development to a slowdown of the Atlantic meridional overturning circulation (AMOC) (Drijfhout et al. 2012; Rahmstorf et al. 2015; Gervais et al. 2018), which observations have suggested is already beginning to occur (Smeed et al.

2014, 2018). The melting of Arctic sea ice and associated increased transport of freshwater from the Arctic into the Labrador Sea can lead to reductions in the AMOC (Jahn and Holland 2013; Böning et al. 2016; Sévellec et al. 2017). Gervais et al. (2018) studied the future development of the NAWH within the Community Earth System Model Large Ensemble (CESM-LE), focusing on local circulation changes. They demonstrated that increased freshwater transport from the Arctic into the Labrador Sea leads to a reduction in Labrador Sea deep convection and a surface cooling. Resulting changes in the local ocean circulation, with a more zonal North Atlantic current and increased transport of this cooler Labrador seawater into the interior of the subpolar gyre, lead to a decreased ocean heat flux convergence in the NAWH region and thus a relative cooling of SSTs.

Previous work on interannual variability in midlatitude SSTs and its impact on atmospheric circulation may provide some basis for understanding how the NAWH might influence atmospheric circulation. Generally, the response to an imposed SST anomaly consists of a linear direct response that is baroclinic (Hoskins and Karoly 1981; Hendon and Hartmann 1982) and a nonlinear equivalent barotropic response in which transient eddy feedbacks play a dominant role (Palmer and Sun 1985; Ting and Peng 1995; Peng and Whitaker 1999; Peng and Robinson 2001; Hall et al. 2001; Deser et al. 2004; Kushnir et al. 2002). This nonlinear equivalent barotropic response typically resembles atmospheric internal variability, for example the North Atlantic Oscillation (NAO) for anomalies imposed in the North Atlantic (Deser et al. 2004; Peng and Robinson 2001). These responses are dependent on the location of the imposed SST anomalies, the anomaly polarity and strength (Hall et al. 2001; Magnusdottir et al. 2004), and the background atmospheric circulation (Ting and Peng 1995; Peng and Whitaker 1999; Hall et al. 2001). As a result, responses to midlatitude SST anomalies may vary by model. An important conclusion drawn in Kushnir et al. (2002), which reviews the atmospheric impacts of interannual SST anomalies, is that the response to midlatitude SST anomalies that occur on an interannual time scale is typically much smaller than atmospheric variability. The notable difference about the NAWH is that it is a sustained change in temperature, which increases the likelihood of a more robust signal.

The North Atlantic Ocean has a defined eddy-driven jet, produced by baroclinic eddy activity in the midlatitudes, that is typically separate from the subtropical jet, produced due to angular momentum transport from the tropics (Lee and Kim 2003). The enhanced baroclinicity associated with gradients in SST is a source of baroclinic wave activity for the North Atlantic storm

track (Nakamura et al. 2004; Brayshaw et al. 2011; Inatsu et al. 2003; Wilson et al. 2009), particularly along the western edge of the Atlantic Ocean (Wilson et al. 2009; Brayshaw et al. 2011) and the subpolar front (Nakamura et al. 2004). Consistent with studies that discuss the nonlinear equivalent barotropic response to SST anomalies (Palmer and Sun 1985; Ting and Peng 1995; Peng and Whitaker 1999; Hall et al. 2001), work that focuses on the influence of anomalies in the SST field or its gradients on storm tracks and jets has also found a strong sensitivity to the location of the SST gradient relative to the mean jet position (Brayshaw et al. 2008; Inatsu et al. 2003; Baker et al. 2017). In particular, Brayshaw et al. (2008) showed that North Atlantic SST gradients located poleward of the subtropical jet produce a poleward shift and enhancement of the eddy-driven jet acting to further separate it from the subtropical jet. However, when these gradients are located close to or equatorward of the subtropical jet they can act to enhance the subtropical jet and shift the storm track equatorward (Brayshaw et al. 2008; Nakamura et al. 2004). The NAWH is located just poleward of the subpolar front, acting to increase the SST gradient already present in this region, and thus may be expected to strengthen the eddy-driven jet.

Future changes to jet structures in response to global climate change have also been a topic of considerable interest (Chang et al. 2012; Harvey et al. 2012; Woollings and Blackburn 2012; Barnes and Polvani 2013; Harvey et al. 2014, 2015; Shaw et al. 2016). The leading mechanisms through which these jets are expected to change are summarized in the review of Shaw et al. (2016) as a tug of war between thermodynamic impacts, such as the increased latent heat release due to tropical convection causing an enhanced temperature gradient aloft, and increased polar temperatures at lower levels from Arctic amplification leading to a decrease in temperature gradients at lower levels. The intermodel spread in jet changes in the Southern Hemisphere is well explained by the relative impacts of the zonal average upperversus lower-level atmospheric temperature gradients, but the situation is more complicated in the Northern Hemisphere (Harvey et al. 2014). In the North Atlantic, projected changes in the winter jet position are modest with a potential poleward shift or eastward extension (Barnes and Polvani 2013; Woollings and Blackburn 2012; Chang et al. 2012) and differences among climate model simulations are large (Harvey et al. 2014).

These studies illustrate the importance of understanding all potential impacts on the North Atlantic jet; however, few studies have focused on the impact of the North Atlantic warming hole. Woollings et al. (2012) demonstrated that changes in the North Atlantic storm

tracks are correlated with changes in the AMOC, which as discussed above is related to the NAWH. They further examined this relationship using a fully coupled simulation with freshwater hosing that produced cooling in the subpolar gyre and an increase in storm track activity (Woollings et al. 2012). In contrast, several studies using imposed SST changes to understand observed or future trends in SSTs have found a limited response to imposed cooling in the subpolar gyre (Ciasto et al. 2016; Harvey et al. 2015; Magnusdottir et al. 2004).

In this study, we are addressing the question of how the development of the NAWH affects atmospheric circulation in the CESM model. Because the impact of SST gradients on atmospheric circulation is very sensitive to the atmospheric base state and location of the SST gradient, the approach taken in this study is to keep all aspects of the simulations as close to the fully coupled CESM-LE experiment as possible. We conduct a series of large-ensemble atmosphere-only experiments forced with SSTs from the multiple CESM-LE coupled model simulations, thus maintaining the large amount of internal variability present in the SST boundary conditions. To understand how the development of the NAWH impacts the atmosphere, experiments are conducted by adding seasonally varying SSTs anomalies within the NAWH region for various time intervals during the twenty-first century and with varying strengths. With the production of a large ensemble of simulations for each experiment we have robust statistics and are able to diagnose the mechanisms responsible for the atmospheric response. In contrast to Ciasto et al. (2016), Harvey et al. (2015), and Magnusdottir et al. (2004) but in keeping with Woollings et al. (2012), we find that the NAWH has a significant influence on atmospheric circulation and the North Atlantic jet. Our results indicate that the impact of the NAWH warrants consideration in order to understand future changes in the Northern Hemisphere atmospheric circulation and the North Atlantic midlatitude jet.

2. Methods

The Community Earth System Model 1.2 (CESM) was employed to conduct a series of large-ensemble experiments to investigate the impact of the NAWH on the atmosphere. The model configuration has active atmosphere and land components but prescribes ocean and sea ice fields. The atmosphere model is the Community Atmosphere Model 5.3 with a horizontal resolution of $0.9^{\circ} \times 1.25^{\circ}$ and 30 vertical levels, and the land model is the Community Land Model 4.5 at the same horizontal resolution. Details regarding the CESM model components can be found in Hurrell et al. (2013)

TABLE 1. List of experiments conducted and their specifications.

| Experiment name | SST modification | Time interval |
|-----------------|-------------------------------|---------------|
| CNTRL10 | _ | 2006–19 |
| CNTRL50 | _ | 2046-59 |
| CNTRL90 | _ | 2086-99 |
| 1KFill50 | +1 K fill | 2046-59 |
| 2XDeep50 | -1 K fill | 2046-59 |
| 2KFill90 | +2 K fill | 2086-99 |
| 2XDeep90 | $-2 \mathrm{K} \mathrm{fill}$ | 2086-99 |

and additional aspects of its representation of climate variability can be found in the CESM1 special issue collection of the *Journal of Climate* (http://journals.ametsoc.org/topic/ccsm4-cesm1).

We have added a new functionality to the CESM prescribed ocean and sea ice configuration to include variable sea ice thickness instead of the default assumption that sea ice is 2m thick when present. This is possible in our experiments because our boundary conditions are from the CESM-LE simulations that output daily sea ice thickness. Sea ice thickness has large spatial variability that impacts the conduction of heat through the sea ice and into the atmosphere, and therefore using variable thickness acts to reduce surface atmospheric temperature biases associated with the constant thickness assumption.

Using this model configuration and radiative forcing from the RCP8.5 scenario, a total of seven prescribed SST and sea ice experiments are conducted, each of which consists of 25 ensemble members. The experiments are conducted over three different time intervals, 2006–19, 2046–59, and 2086–99, and they consist of "control" runs and "modified" runs where SSTs are altered over the North Atlantic. The prescribed SST and sea ice are based on output from CESM-LE RCP8.5 fully coupled simulations over the corresponding time intervals with an approximately 1° horizontal resolution and daily temporal resolution. See Kay et al. (2015) for details regarding the CESM-LE experiment. A summary of the experiments performed here is provided in Table 1.

For each control experiment, a set of hybrid runs is branched from the restart files of individual CESM-LE ensemble members. The prescribed boundary conditions are the daily SST and sea ice output from the corresponding ensemble member over the corresponding 14-yr period. For example, the first ensemble member in the control experiment over the 2006–19 time interval is branched from the first ensemble member of the CESM-LE in 2006. This simulation is then run over the 2006–19 time interval with prescribed SST and sea ice conditions from the same CESM-LE ensemble member over the 2006–19 time interval. This procedure

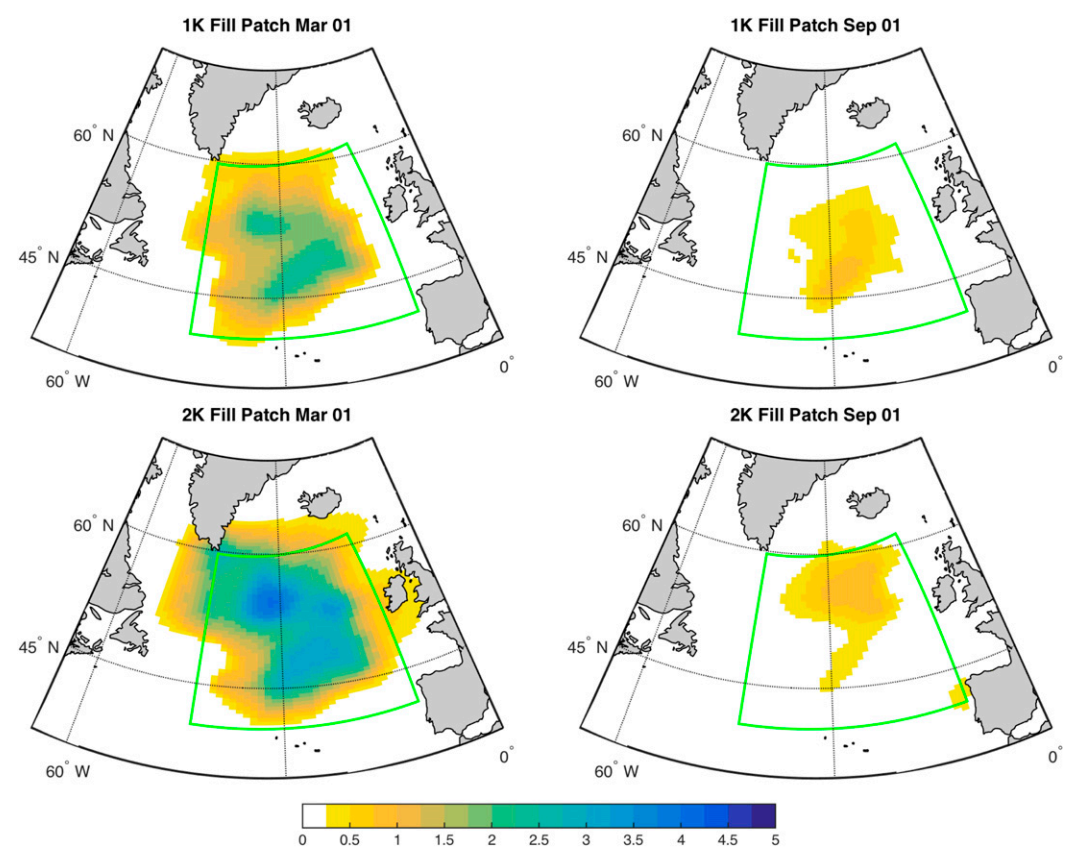


FIG. 1. Experiment fill patches for the (top) 2050s and (bottom) 2090s, for (left) 1 Mar and (right) 1 Sep. The green box represents the NAWH region in which the SSTs are altered. Patches that extend beyond the box occur when patch values are positive at the box edge and are linearly interpolated to zero away from the boundary to smooth the patch edges.

is repeated for 25 ensembles members per experiment. This is a subset of the total number of ensemble members available from the CESM-LE due to limitations in computational resources. The control experiments over the 2006–19, 2046–59, and 2086–99 time intervals will be subsequently referred to as CNTRL10, CNTRL50, and CNTRL90. All subsequent analysis of these simulations neglects the first four years of the simulations to account of any adjustment to the changes in model configuration and boundary conditions.

The SSTs prescribed in the CNTRL simulations are identical to those in the fully coupled CESM-LE experiments; however, the lack of coupling in these experiments could be important both in determining the mean atmospheric state and the response to the NAWH. Examining the seasonal ensemble mean turbulent heat fluxes in the CNTRL compared to the CESM-LE experiments reveals some significant differences on the order of $10 \, \mathrm{W \, m^{-2}}$ (see Fig. S1 in the online supplemental material). As a result, we cannot rule out the potential importance of coupling in this process, although the role of the NAWH in modulating turbulent

heat fluxes is similar between the CNTRL and CESM-LE simulations (Fig. S2).

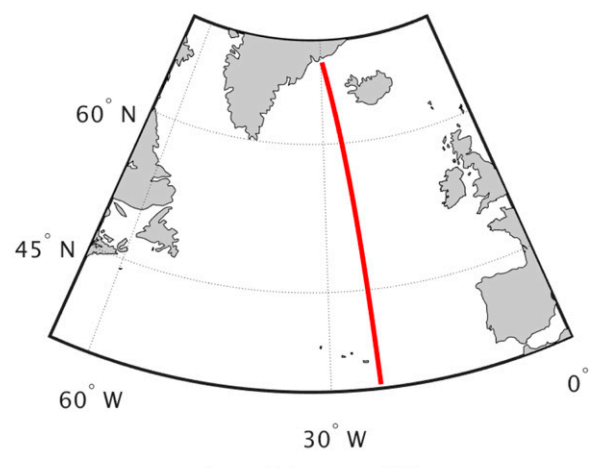
To produce the boundary conditions for the modified experiments, we first create two seasonally varying fill patches, one each for the 2050-59 and 2090-99 analysis periods. In general, SSTs averaged over the entire North Atlantic are 1 K higher in the 2050–59 period (2050s) and 2 K higher in the 2090–99 period (2090s) compared to the 2010-19 period (2010s). The two fill patches are produced to represent the magnitude of the deficit in warming within the NAWH region (shown as a green box in Fig. 1) in the 2050s and 2090s with respect to 1-K and 2-K thresholds respectively. The NAWH region is defined such that it encapsulates the majority of the NAWH but omits sections within the Labrador Sea and close to the Greenland coast where the formation of seasonal sea ice would be a factor (Fig. 1). To construct the fill patches, we begin by computing the ensemble decadal average of SSTs for each day of the year in the 2010s, 2050s, and 2090s. For each day of the year and at each location within the NAWH region, if the SSTs in the 2050s are less than 1 K higher than they were in the

2010s the fill patch is equal to the magnitude of this difference. The same procedure is applied to create a 2090s fill patch but using a 2-K threshold. Values of the fill patch at the edges of the NAWH domain are then linearly interpolated down to zero over the distance of 5 grid points for the 2050s and 10 grid points for the 2090s in order to avoid abrupt SST gradients that could produce spurious baroclinic zones. The patches are thus constructed such that when added to the control SST they either fill or deepen the warming hole while leaving SSTs outside the warming hole unchanged.

The resulting fill patches have a large seasonality with greater values in the spring/winter and smaller values in the fall/summer. Examples of the 1 March and 1 September fill patches for the 2050s and 2090s are shown in Fig. 1. These example days illustrate the large seasonality and the smoothness of the boundaries of the fill patches for both the 2050s and 2090s.

The modified experiments are conducted as for the control experiments but with the addition or subtraction of these seasonally varying fill patches. Two additional sets of experiments, "filled" or "deepened," are conducted for each of the 2046–59 and 2086–99 time intervals. The boundary conditions for the filled experiments are created by adding seasonally varying fill patches to each year of the control simulation's SSTs, whereas the deepened experiments are instead created by subtracting the fill patches. The 2046–59 experiments are produced using the seasonally varying 1KFill patch and are referred to as the 1KFill50 for the filled experiment and 2XDeep50 for the deepened experiment. Similarly, for the 2086–99 experiments the 2KFill patch is employed and the filled experiment is referred to as 2KFill90 and the deepened experiment as 2XDeep90.

Cross sections of annual decadal ensemble mean SST for each experiment illustrate how the addition or subtraction of these fill patches does indeed result in SSTs that follow the shape of the earlier period but with a net average increase in SST for the filled experiments and decrease in SSTs for the deepened experiments (Fig. 2). An important feature of the SSTs in this region is the existence of the subpolar SST front, which can be seen in the light gray CNTRL10 simulation in Fig. 2 as the large gradient in SST centered near 50°N with colder temperatures to the north and warmer to the south. The NAWH is a relative cooling confined to the subpolar gyre resulting in a further enhancement of the subpolar front gradient, as can be seen in the cross section of CNTRL50 and CNTRL90 SST (Fig. 2). In this context we see how the 1KFill50 and 2KFill90 experiments maintain the same SST gradients as in the CNTRL10 experiments but with an average SST increase, whereas the 2XDeep50 and 2XDeep90 experiments further enhance the subpolar SST front (Fig. 2). Part of the



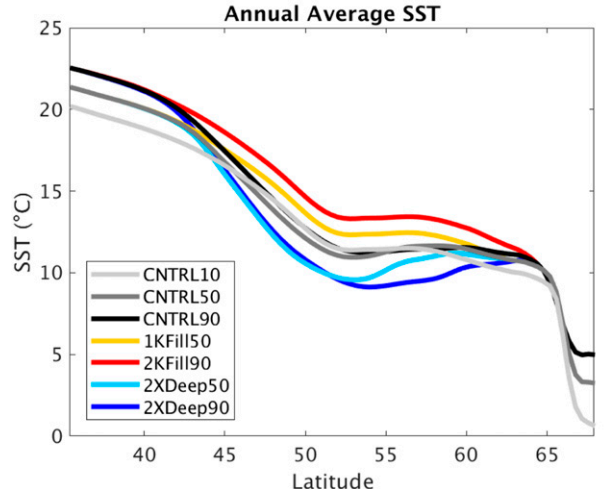


FIG. 2. (bottom) Annual ensemble average SST for each experiment through (top) a north-south cross section with location depicted as the red line at approximately 25°W and from 30° to 70°N.

development of the NAWH is a more zonal North Atlantic Current (Gervais et al. 2018), which also results in a southward shift of the subpolar SST front, particularly in the eastern portion of the basin. This can also be seen in the SST cross sections (Fig. 2). Seasonal cross sections are provided in Fig. S3 for reference.

3. Results and discussion

a. Atmospheric response to the NAWH

The seasonal mean atmospheric response to the NAWH is assessed by quantifying seasonal ensemble mean differences between experiments (Figs. 3 and 4). These differences are all calculated with respect to the filled experiment; for example, the CNTRL50 – 1KFill50 difference represents the atmospheric impact of the lack of warming in the North Atlantic SST associated with the NAWH, and will subsequently be referred to as the

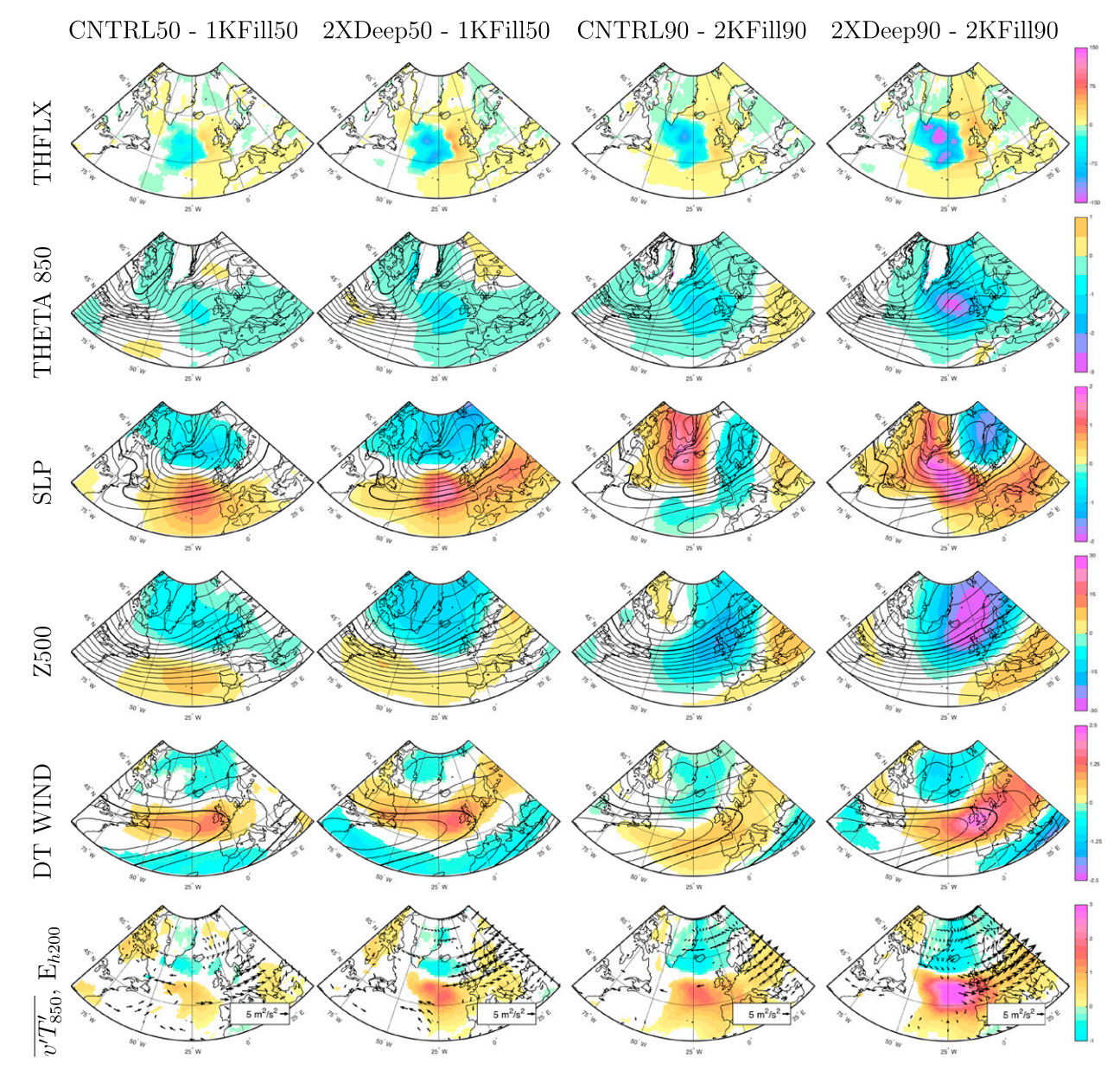


FIG. 3. December–February seasonal ensemble mean differences between experiments for turbulent heat flux (THFLX; W m⁻²), potential temperature at 850 hPa (THETA850; K), sea level pressure (SLP; hPa), 500-hPa geopotential height (Z500; m), wind speed on the dynamic tropopause (DT WIND; m s⁻¹), and $\overline{v'T'}$ at 850 hPa ($\overline{v'T'}_{850}$; K m s⁻¹; colors) and horizontal **E** vector at 200 hPa (**E**_{h.200}; m² s⁻²; arrows). 1KFill and 2KFill seasonal ensemble means for the 2050–59 and 2090–99 experiments respectively are shown in black contours on the THETA850, SLP, Z500, and DT WIND plots with bold contours for reference at 270 K, 1016 hPa, 5400 m, and 30 m s⁻¹ respectively. Only significant values at the 5% significance level as computed using a two-tailed *t* test are shown; vectors are shown if either of the zonal or meridional component is significant.

"response" to the NAWH. Similarly, the 2XDeep50 – 1KFill50 difference will be referred to as the response to the twice deepened warming hole.

The turbulent heat flux response to the NAWH is a collocated reduction in the turbulent heat flux from the ocean to the atmosphere due to the cooler ocean temperatures (Fig. 3). This turbulent heat flux response varies approximately linearly with respect to the SST difference

between experiments, for example December–February (DJF) CNTRL50 – 1KFill50 has a minimum turbulent heat flux of $-50 \,\mathrm{W\,m^{-2}}$ compared to $-100 \,\mathrm{W\,m^{-2}}$ for 2XDeep50 – 1KFill50 (Fig. 3). Similar results are seen between seasons with DJF and March–May (MAM) having the largest SST differences and the largest turbulent heat flux differences between experiments (Figs. 3 and 4) and vice versa for the September–November

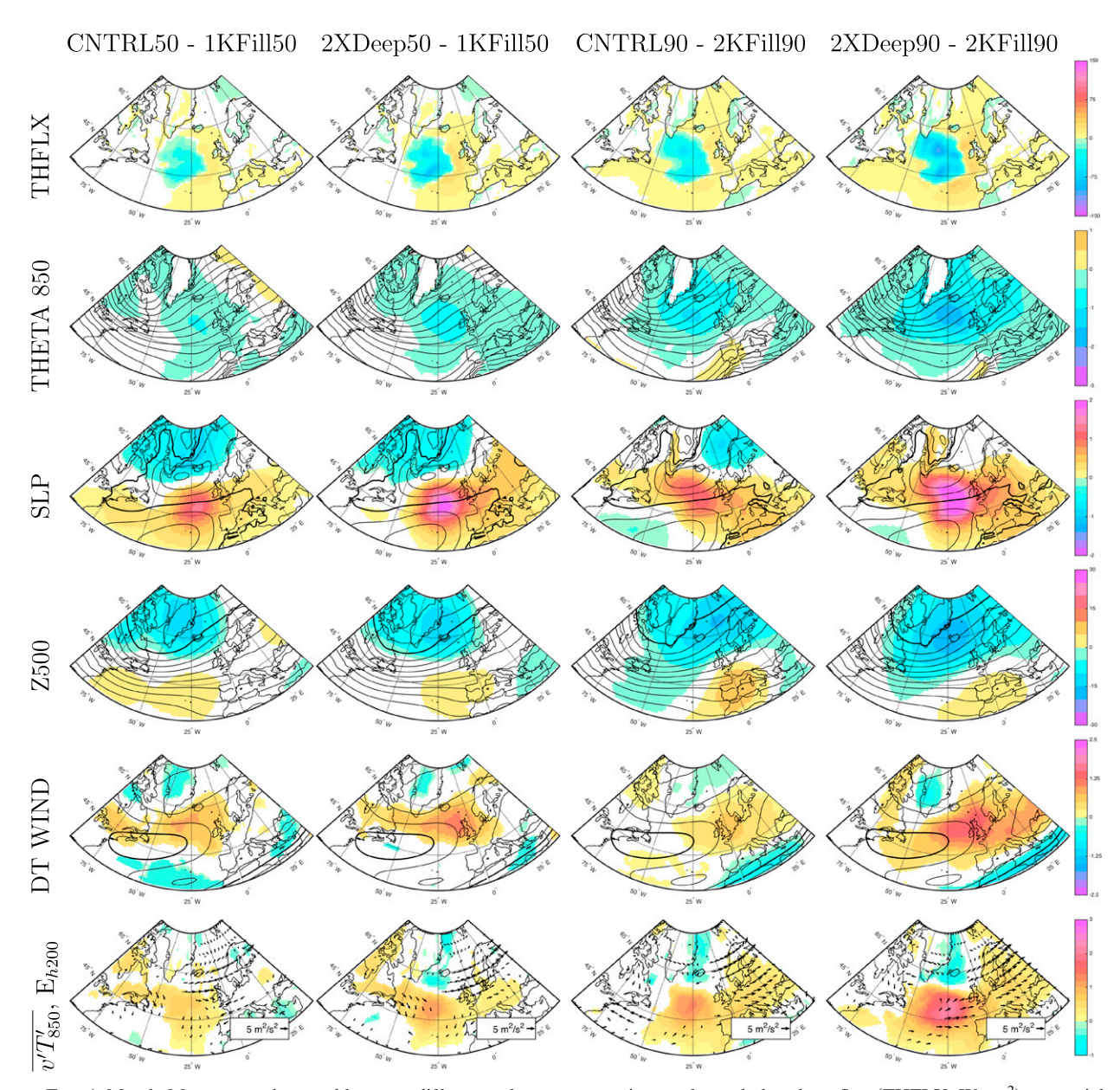


FIG. 4. March–May seasonal ensemble mean differences between experiments for turbulent heat flux (THFLX; W m $^{-2}$), potential temperature at 850 hPa (THETA850; K), sea level pressure (SLP; hPa), 500-hPa geopotential height (Z500; m), wind speed on the dynamic tropopause (DT WIND; m s $^{-1}$), and v'T' at 850 hPa ($v'T'_{850}$; K m s $^{-1}$; colors) and horizontal **E** vector at 200 hPa ($\mathbf{E}_{h,200}$; m 2 s $^{-2}$; arrows). 1KFill and 2KFill seasonal ensemble means for the 2050–59 and 2090–99 experiments respectively are shown in black contours on the THETA850, SLP, Z500, and DT WIND plots with bold contours for reference at 270K, 1016 hPa, 5400 m, and 30 m s $^{-1}$ respectively. Only significant values at the 5% significance level as computed using a two-tailed t test are shown; vectors are shown if either of the zonal or meridional component are significant.

(SON) and July-August (JJA) seasons (Figs. S4 and S5). North and downstream of this reduction in turbulent heat flux we see a relative cooling of potential temperatures that is particularly large in the DJF and MAM seasons when the turbulent heat fluxes are greatest (Figs. 3 and 4).

When examining the impact of the NAWH on the dynamical fields of sea level pressure (SLP), 500-hPa

geopotential height (Z500), and wind speed on the dynamic tropopause [defined as the 2-PVU (1 PVU = $10^{-6} \, \text{K kg}^{-1} \, \text{m}^2 \, \text{s}^{-1}$) surface], we begin to see differing responses with the depth of the warming hole, the time period, and the season. In DJF of the 2050s experiments, the response to the NAWH is a dipole in SLP with localized higher SLP close to the location of the turbulent heat flux anomalies and a lower SLP to the north

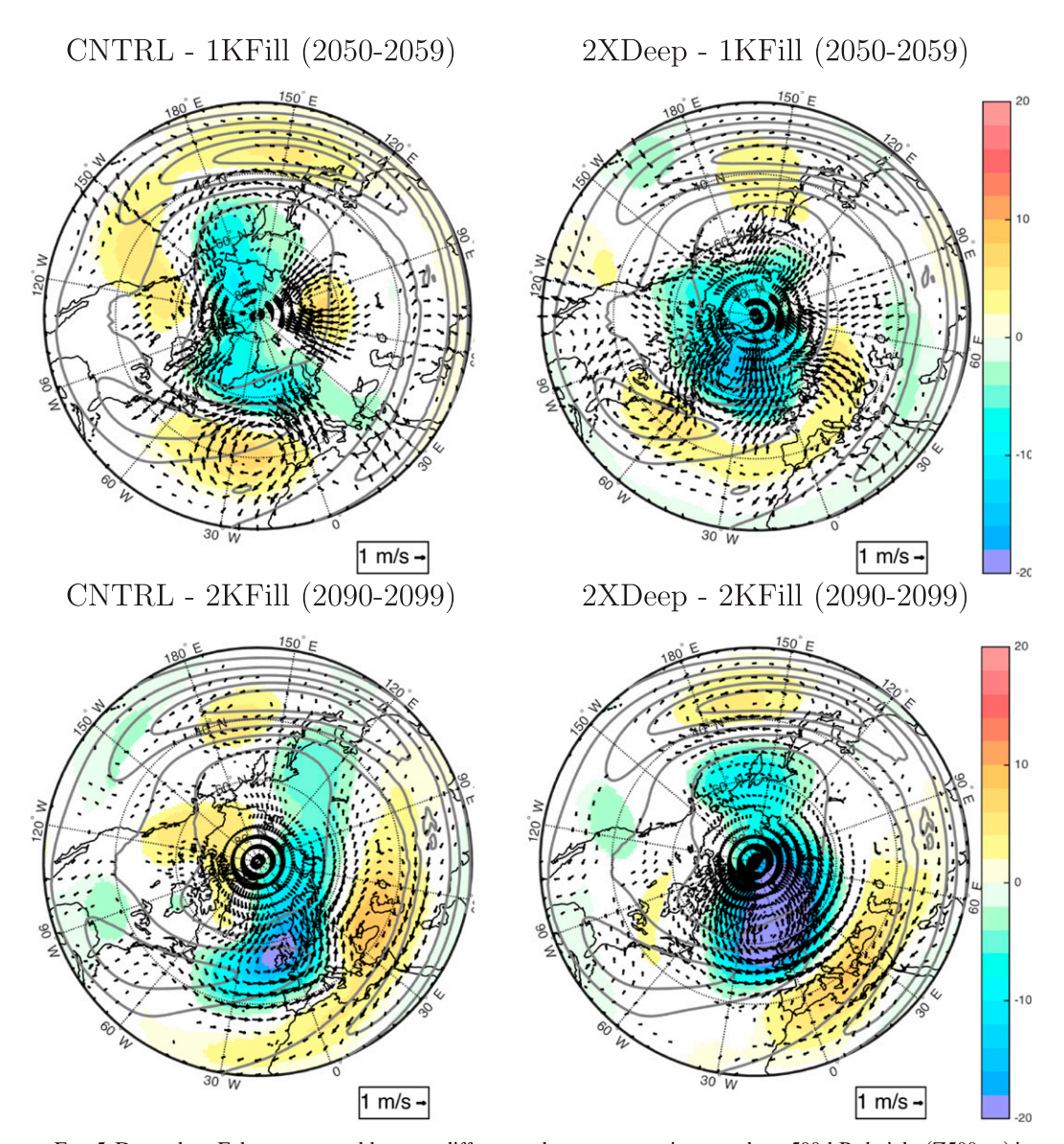


Fig. 5. December–February ensemble mean differences between experiments where 500-hPa height (Z500; m) is in color and wind velocity on the dynamic tropopause is in vectors. The wind speed on the dynamic tropopause of the 1KFill or 2KFill experiment for the 2050s and 2090s experiments, respectively, are also plotted in gray in order to provide a reference of the mean jet location. Only significant values at the 5% significance level as computed using a two-sided t test are shown and for vectors are assigned if either zonal or meridional component are significant.

(Fig. 3). The 500-hPa height response is a dipole flanking the NAWH, bearing some resemblance to the SLP response but shifted slightly southward. Differences in the dynamic tropopause wind speed show an elongation and increase in the strength of the North Atlantic jet that is consistent with a geostrophic balance between the North Atlantic jet and the geopotential heights.

The response to a deepened warming hole in the 2050s (2XDeep50 – 1KFill50) for DJF is similar to the CNTRL50 – 1KFill50 difference but with a stronger

SLP response over the NAWH and a broader longitudinal extent of the dynamic tropopause wind speed and Z500 responses (Fig. 3). When looking at these changes hemispherically, it is interesting to note that the response in the CNTRL50 – 1KFill50 shows lower Z500 in both the Icelandic low and the Aleutian low with increases in wind speed on the dynamic tropopause in both the North Atlantic and North Pacific jets (Fig. 5). As the North Atlantic response elongates longitudinally in the 2XDeep50 – 1KFill50 difference the change in

geopotential height begins to resemble more of an annular mode type pattern and the response in the Pacific jet is reduced.

The DJF response of the dynamical fields in the 2090s is quite different from the 2050s (Fig. 3). For the CNTRL90 - 2KFill90 response, the dynamic tropopause wind speed shows an equatorward strengthening and an elongation of the North Atlantic jet over northern Europe and Russia with coinciding and roughly equivalent barotropic changes in the Z500 and SLP fields. Although there is some localized positive SLP response to the NAWH in the 2090s it is shifted significantly northward and over Greenland. The DJF response to a twice deepened warming hole in the 2090s is an elongation of the North Atlantic jet, without any equatorward strengthening, more similar to the 2050s response but shifted farther downstream over Europe (Fig. 3). There is an equivalent barotropic Z500 and SLP response flanking this jet, again located downstream of the NAWH region over Europe. Directly over and slightly downstream of the NAWH heat flux anomalies we see a strong local positive SLP response.

To diagnose the role of the storm track responses to changes in SST and their impact on the North Atlantic jet, we follow the diagnostic method proposed by Hoskins et al. (1983). We examine the lower-troposphere eddy heat transport $\overline{v'T'}$ at 850 hPa $(\overline{v'T'}_{850})$, a measure of the vertical eddy activity propogation, and the horizontal component of the upper-troposphere **E** vector:

$$\mathbf{E}_h = (\overline{v'^2 - u'^2}, -\overline{u'v'}),\tag{1}$$

which allows for estimating the eddy momentum forcing of the zonal time-mean flow. A 3–8-day high pass filter is applied to the u (zonal wind component), v (meridional wind component), and T (temperature) prior to the calculation of $\overline{v'T'}$ and \mathbf{E}_h in order to isolate the influence of baroclinic transient eddy activity on the zonal flow. Positive $\overline{v'T'}$ values in the lower troposphere are indicative of westward tilted eddies with height and upward propagation of eddy activity. The divergence of the \mathbf{E}_h vector in the upper troposphere provides information on the transient eddy forcing of the zonal mean flow via momentum transfer. A positive divergence indicates an eddy-forced, eastward acceleration of the mean flow. The analysis presented here with $v'T'_{850}$ and \mathbf{E}_h divergence at 200 hPa ($\mathbf{E}_{h,200}$) thus provides information about the baroclinic transient eddy response and subsequent transfer of eddy energy into the mean flow.

The DJF $\overline{v'T'_{850}}$ response in the 2050s (CNTRL50 – 1KFill50) shows a region of enhanced storm activity

consistent with an enhanced surface baroclinic zone at the southern edge of the warming hole (Fig. 3). Downstream of this enhanced low-level eddy activity is a divergence of the horizontal E vector components aloft implying that this enhanced eddy activity is providing energy to the mean flow downstream of the NAWH. This is consistent with the enhanced strength of the jet stream seen in the dynamic tropopause wind speed figures. When the NAWH is deepened, shown in the 2XDeep50 - 1KFill50 differences (Fig. 3), we see a similar DJF response but the transient eddy mean interaction shown by the $\mathbf{E}_{h,200}$ divergence is stronger and shifted farther downstream. This is consistent with the response of the dynamic tropopause wind speed where the North Atlantic jet is further strengthened both upstream and downstream of the imposed SST differences and the geopotential height differences are similarly broadened in the zonal direction.

The 2090s experiments exhibit a much stronger $v'T'_{850}$ response in DJF and the $\mathbf{E}_{h,200}$ response is located even farther downstream (Fig. 3). This coincides with the enhanced dynamic tropopause wind speed over northern Europe and Russia (Fig. 5). Of note for the CNTRL90 – 2KFill90 difference is that the positive jet response is on the equatorward side of the mean jet location. The positive and negative Z500 and SLP dipoles associated with the enhanced jet are similarly shifted downstream leading to a very different local SLP response over the NAWH region.

When the warming hole is deepened in the 2XDeep90 - 2KFill90 response we see a further increase in $\mathbf{E}_{h,200}$ divergence and the jet is strengthened and elongated (Fig. 3). There is a consistent Z500 and SLP dipole response flanking this change in the jet strength that is farther downstream than the turbulent heat flux response. We see a stronger positive SLP response located just north and slightly downstream of the turbulent heat flux response, consistent with the stronger turbulent heat flux response and the equivalent barotropic response located downstream instead of impacting the NAWH region directly.

There are many similarities between the magnitude of the SST differences and the atmospheric response between the DJF and MAM seasons (Figs. 3 and 4). This is particularly true for the turbulent heat flux and 850-hPa potential temperature responses, which, similar to DJF, are approximately linear with respect to the SST difference. There is also a local increase in $v'T'_{850}$ over the NAWH region and a downstream increase in $\mathbf{E}_{h,200}$ divergence aloft (Fig. 4). These regions of enhanced input of eddy energy into the mean flow coincide with a poleward strengthening and elongation of the North Atlantic jet. As was the case in DJF, the impact on the

jet shifts farther downstream as the warming hole deepens. This is seen in both the response to the twice deepened NAWH compared to the NAWH, and in the 2090s relative to the 2050s. There is also a dipole in Z500 response with negative anomalies poleward and positive anomalies equatorward of the jet response. The SLP response, however, is less clearly equivalent barotropic; instead, the localized positive SLP response over the NAWH is more robust in MAM than in DJF. In general, the transient eddy-driven jet is weaker in the spring, which could result in a weaker eddy-mean flow interaction response in MAM compared to DJF.

In SON the imposed SST differences are smaller and the North Atlantic jet is weaker. The response in this season is typically a smaller localized increase in SLP directly over or shifted slight downstream of the NAWH (Fig. S4). The response in terms of $\overline{v'T'_{850}}$, $\mathbf{E}_{h,200}$, dynamic tropopause wind speed, and Z500 are limited except for the 2XDeep90–2KFill90 case where there is a small response similar to that in MAM (Fig. 4).

The response in JJA is characterized by a similar increase in SLP over the NAWH region (Fig. S5). The upper-level response varies somewhat from the other simulations with no equivalent barotropic response but rather a small low in Z500 downstream of the high SLP response and some increased dynamic tropopause wind speed on the southern flank of this Z500 response. In general, this response is quite weak and resembles a baroclinic Rossby wave. These results are consistent with previous work that examined the impact of SST anomalies associated with Atlantic multidecadal variability in observations (Ghosh et al. 2017) and the slowdown of the AMOC in CMIP5 models (Haarsma et al. 2015) during the JJA season.

b. Proposed mechanisms

The results presented above allow us to formulate an understanding of the processes involved in the atmospheric response to the NAWH. In general, we can see two types of response, a direct linear response and a transient eddy forced response. The total response to the NAWH is a combination of the two, which each have different strengths depending on the season, time period, and warming hole depth. These two types of responses are consistent with previous work on the impacts of interannual SST variability in the midlatitudes summarized in Kushnir et al. (2002).

1) DIRECT LINEAR RESPONSE

The first mechanism is consistent with a steady linear response to shallow heating in the midlatitudes as has been demonstrated in prior studies using linearized models (Hoskins and Karoly 1981; Hendon and Hartmann

1982; Held 1983; Kushnir et al. 2002). The atmospheric response to a heating anomaly is dependent on both the latitude and height of the forcing (Hoskins and Karoly 1981), where the NAWH is best characterized as a shallow midlatitude thermal forcing. The response to a shallow positive heating anomaly in the midlatitudes is characterized by a downstream shifted low in sea level pressures, positive temperatures (Hendon and Hartmann 1982; Hoskins and Karoly 1981), and northerly advection over the heating anomaly (Hoskins and Karoly 1981).

In the case of the NAWH, we have an imposed SST difference that leads to a decrease in turbulent heat flux, or a local cooling, consistent with a shallow cooling that decreases with height. We therefore expect a positive SLP anomaly located just downstream of this imposed cooling and a baroclinic geopotential height response that is positive in the lower troposphere and negative in the upper troposphere. A schematic of this response is provided in Fig. 6.

In nearly all experiments, we do see a local high in SLP and reduced potential temperature at 850 hPa above or shifted slightly downstream of the turbulent heat flux differences. The strength of this response is approximately linear with the imposed SST difference. The baroclinic structure with height is found in some simulations but is less robust. The direct linear response is most apparent in seasons where the eddydriven jet is weak such that there is a limited transient eddy forced response or when the transient eddy forced response occurs farther downstream than local direct response.

Kushnir et al. (2002) summarized that for interannual variability the direct linear response will rarely be relevant in the extratropics because the response is much smaller than atmospheric variability. In the case of the NAWH forcing, we have a constant change in SST that is best described as a change in the boundary condition. With this long-term steady forcing and the time and ensemble averaging conducted here, internal variability is filtered out and the response is detected. This is similar to how the weak linear response was detected in earlier studies cited in Kushnir et al. (2002).

2) Transient eddy forced response

The second response mechanism involves the interaction between the perturbed baroclinic eddies in the storm track and the mean flow. The NAWH is located on the poleward flank of the subpolar front and, as seen in Fig. 2, acts to further enhance the polar SST front. The polar SST front is a source of baroclinicity for the North Atlantic storm track (Nakamura et al. 2004), making the location of the NAWH optimal for impacting baroclinic eddy activity.

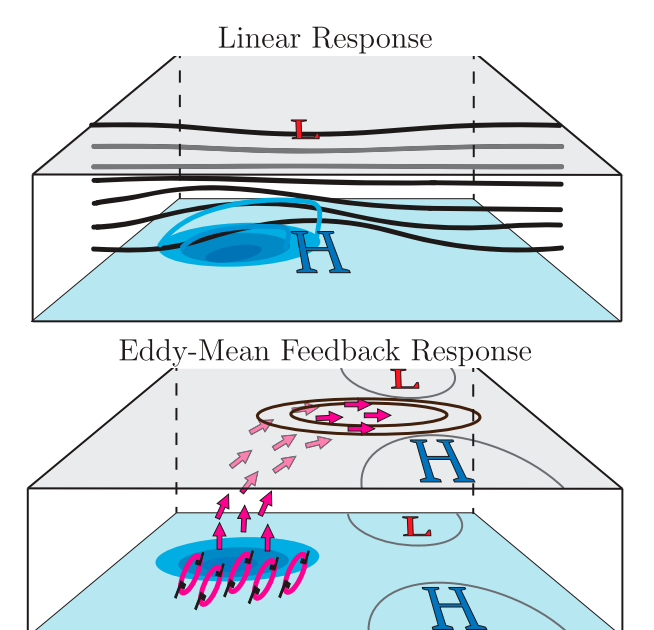


FIG. 6. Schematics of (top) the direct linear response to the NAWH and (bottom) the indirect transient eddy forced response. The blue surface represents the ocean, the gray surface the upper troposphere, and the blue ovals the NAWH. For the linear response, atmospheric cooling that decreases with height is identified by the blue lines, the black lines illustrate changes in geopotential height tilting westward with height, and high and low pressure are indicated with letters. For the transient eddy forced response, the transient eddy activity is indicated with pink ellipses and pink arrows that indicate upward and eastward eddy activity propagation. Changes in jet level winds are indicated with black ellipses and high and low pressures at the surface and upper levels are shown as gray circles and corresponding letters. Here the impact of transient eddy forcing is depicted as being downstream of the imposed SST anomaly; however, the response could occur closer to the imposed SST anomaly.

The NAWH enhanced surface baroclinicity leads to an enhancement of transient baroclinic eddy activity near the surface, which propagates vertically and horizontally downstream of the NAWH. In the upper troposphere, this enhanced eddy activity acts to enhance the eddy-driven jet. Consistent with geostrophic balance, there is reduced Z500 poleward and increased Z500 equatorward of these jet changes. The total response is equivalent barotropic, projecting to the surface. This is reminiscent of the NAO, the leading mode of internal variability in the region, although the location of the response shifts farther downstream as the baroclinic eddy activity increases. A schematic of this process is provided in Fig. 6.

The transient eddy forcing mechanism tends to dominate over the direct linear response when the responses are collocated. However, the transient eddy forced response shifts farther downstream as the NAWH becomes larger, while the direct linear response remains localized close to the SST anomalies. As a result, the two responses

are more geographically separated and easier to identify when the NAWH is larger, as is the case for example in the 2XDeep90 – 2KFill90 differences during DJF.

The seasonality of the NAWH is such that the warming hole is greatest during DJF and MAM and smallest during SON and JJA (Fig. 1). The transient eddy forced response is present in both DJF and MAM when there is a pre-existing strong eddy-driven jet and large enough SST anomalies to produce the response, but is largest in DJF when the jet is strongest. There is also, a small transient eddy forced response in the SON 2KFill90 – 2XDeep90 difference (Fig. S4), as the NAWH SST gradients become larger in the latter time period and with a twice deepened warming hole (Fig. 2).

This mechanism producing the response is similar to the transient eddy-mean flow interaction mechanisms described in previous studies on the impacts of interannual SST variability on the atmospheric circulation (Ting and Peng 1995; Peng and Whitaker 1999; Peng and Robinson 2001; Hall et al. 2001; Deser et al. 2004; Kushnir et al. 2002). Our results also show that the NAWH response shifts downstream with time period and warming hole strength. The North Atlantic jet acts as a waveguide in the region (Hoskins and Ambrizzi 1993) and as such refraction of eddy activity along the mean jet core would translate the transient eddy forced response farther downstream when the jet is stronger. Because the North Atlantic jet is stronger in the 2090s than the 2050s the transient eddy forced response to the NAWH is farther downstream in the 2090s compared to the 2050s. Similarly, because the warming hole causes an enhancement of the North Atlantic jet, the twice deepened NAWH leads to a transient eddy forced response that is farther downstream than the NAWH response.

Many previous studies have noted that the background atmospheric state is an important factor in determining the response to SST anomalies and gradients, in particular that the location of the SST anomaly relative to the mean jet location is important (Ting and Peng 1995; Peng and Whitaker 1999; Hall et al. 2001; Brayshaw et al. 2008; Inatsu et al. 2003; Baker et al. 2017). In the case of the NAWH, the pre-existing gradient in SST across the subpolar front is enhanced, which explains why the transient eddy forcing response is typically a strengthening of the North Atlantic jet without any shifting. It is worth noting that because the North Atlantic jet has a southwest-northeast tilt, the zonal mean wind speed over the North Atlantic might appear as a poleward shift. Given the mechanism for the NAWH formation described in Gervais et al. (2018), the NAWH should always be confined to the subpolar gyre and thus result in an enhanced SST gradient within the subpolar front. If the mechanisms for the NAWH are

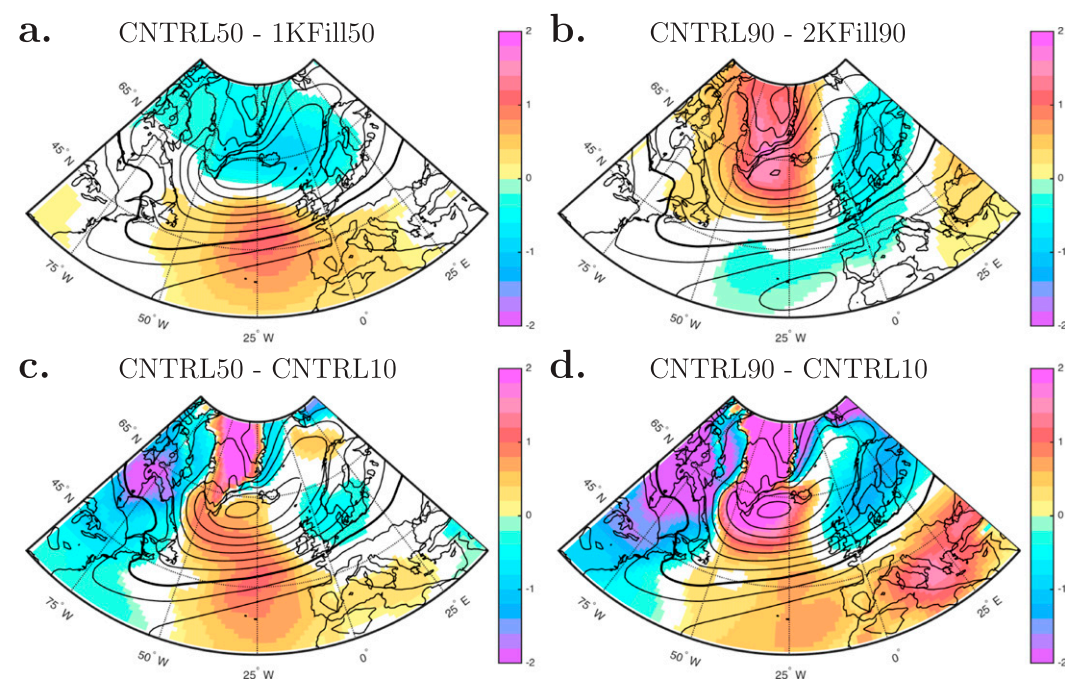


FIG. 7. December–February seasonal ensemble mean differences in sea level pressure (hPa) between (a) CNTRL50 and 1KFill50, (b) CNTRL90 and 2KFill90, (c) CNTRL50 and CNTRL10, and (d) CTNRL90 and CNTRL10. Seasonal mean differences are in color with only significant values at the 5% significance level as computed using a two-sided *t* test are shown. For reference, 1KFill50, 2KFill90, CNTRL10, and CNTRL10 seasonal ensemble means in (a)–(d), respectively, are shown in black contours with the 1016-hPa contour in bold.

consistent between models and given that the eddydriven jet is typically geographically tied to the Gulf Stream and the subpolar front, one might therefore expect various models to have NAWH SST anomalies in a similar position relative to their own model's storm track.

The location and strength of the subtropical jet may also be important for this mechanism. The North Atlantic typically exists in a regime in which there are separate subtropical and eddy-driven jets because the eddy-driven jet is strong relative to the subtropical jet (Lee and Kim 2003; Brayshaw et al. 2008). Generally, if the subtropical jet is stronger than the eddy-driven jet, as is more common in the Pacific, eddy momentum can feed into a single subtropical jet instead of a separate eddy-driven jet (Nakamura et al. 2004; Lee and Kim 2003). There are several factors influencing future changes in the subtropical jet that, depending on the relative strengths of these changes, could result in changes in the transient eddy forcing mechanism. Because the subtropical jet is stronger in the 2090s than in the 2050s the frequency of a single jet regime may be higher, leading to enhanced eddy momentum flux that strengthens the single subtropical jet equatorward of the mean eddy-driven jet.

There are some indications of this deposition of eddy energy in the subtropical North Atlantic jet in the CNTRL90 – 2KFill90 difference in DJF where we see an equatorward jet enhancement in the North Atlantic. When the warming hole is deepened in the 2090s (2XDeep90 – 2KFill90), we again see an extension of the North Atlantic jet, which may be the result of these eddy momentum fluxes once again strengthening the eddy-driven jet as it becomes stronger relative to the subtropical jet (Fig. 3).

c. Comparison to total climate change forcing

To place the atmospheric response to the NAWH in context, we next compare it to the total climate change response. In the filled experiments, we are imposing an SST anomaly so as to remove the development of the warming hole that occurs between the 2050s or 2090s and the 2010s. Comparing the total climate change response, defined as the difference between the CNTRL50 or CNTRL90 and the CNTRL10 experiments, to the filled experiment responses thus allows us to assess the portion of the total climate change response that may be caused by the development of the warming hole.

Over the North Atlantic, the DJF mean impact of climate change from the 2010s to the 2050s has a large positive SLP anomaly that is of equal magnitude to the high SLP response to the NAWH in the 2050s (Fig. 7). In the total climate change response, this region of high

SLP extends into the Labrador Sea, which could be related to the NAWH extension in this region that we have omitted in our development of the NAWH patch. The total global climate change signal also includes lower SLP over much of the Arctic, which differs from the NAWH response and may be the result of future sea ice loss. In the 2090s there is also a strong similarity in pattern and magnitude of the climate change response and the NAWH response in regions where the NAWH has a significant impact. In particular, the high SLP response to the NAWH south of Greenland and the low SLP response over northern Europe is present and of a similar magnitude in the total climate change response. These results imply that the NAWH plays a significant role determining climate change impacts on sea level pressure over the North Atlantic and the adjacent European continent.

Significant changes in the atmospheric jets are expected with global climate change due to changes in the equator to pole temperature gradients at the upper and lower levels of the troposphere (Harvey et al. 2014; Shaw et al. 2016). In the full climate change response, the largest changes are significant increases in dynamic tropopause wind speed in the subtropical jet south of 35°N that are much larger than the impacts of the NAWH. Where there is a significant response to the NAWH in the North Atlantic and North Pacific, the magnitude of this NAWH response is roughly half that of the full global climate change response. The DJF NAWH response in the 2050s occurs in both the Atlantic and Pacific jets acting to shift them poleward and extend them eastward, as can be seen by the dipole in dynamic tropopause wind speed anomalies (Fig. 8). The 2090s NAWH response in DJF differs somewhat from the 2050s response with an increase in the jet strength slightly equatorward, a large region of increased strength spanning across Europe and Russia, and a decrease over northern Africa and central Asia (Fig. 8).

One factor is that is not considered in this study is how future changes in SSTs outside of the NAWH region could also have implications for the NAWH response. For example, Harvey et al. (2015) find that SSTs in the subpolar gyre covary with those in the Greenland–Iceland–Norwegian Seas. Gervais et al. (2018) (their Fig. 1) show an increase in SST in the subtropical gyre as a response to global warming that acts to enhance the SST gradient along the subpolar front. Such changes in the subtropical gyre SSTs would further increase the transient eddy forcing mechanism and could partly explain why the total global climate change response bears a close resemblance to the NAWH response but is nearly twice as strong (Fig. 8). The result could be transient eddy forced responses occurring sooner in the

total climate change response than in the NAWH response. This might explain the increase in dynamic tropopause wind speed over Russia that is found in the NAWH response in the 2090s but begins to occur in the full climate response in the 2050s.

4. Conclusions

This study examines the impact of a warming deficit in North Atlantic SSTs on atmospheric circulations within future climate simulations of the CESM. A series of prescribed SST and sea ice experiments are constructed using the CESM-LE simulations with the NAWH either filled in or deepened. The results show a significant atmospheric response to these changes in SST that spans the entire hemisphere with most notable impacts on local sea level pressure, tropospheric temperature, and the North Atlantic jet. The atmospheric response to the NAWH is found to depend on the strength of the SST gradient in the subtropical gyre, the time period of study, and the season. The magnitude of the NAWH response in SLP and winds on the dynamic troposphere is comparable to the total global climate change signal over the North Atlantic, an indication of the importance of this mechanism.

The atmospheric response to the NAWH in the CESM model can be described as a combination of two mechanisms: a direct linear response and a transient eddy-forced response. The direct linear response is baroclinic, consisting of a shallow cooling that decreases with height and the development of a local surface high pressure anomaly shifted slightly downstream of the SST anomaly. The transient eddy-forced response develops as a result of enhanced surface baroclinicity along the subpolar front due to cooling in the NAWH. This leads to enhanced transient eddy activity that propagates vertically and downstream of the SST anomaly and acts to strengthen the eddy-driven jet. Jet enhancement from this transient eddy-mean flow interaction results in the development of equivalent barotropic highs and lows on the equatorward and poleward side of the jet enhancement respectively. As the NAWH deepens and this surface baroclinicity is greater, the upper-level response shifts farther downstream.

The experiments in this study directly isolate the impacts of SSTs associated with the NAWH. However, one aspect that cannot be ascertained due to the experimental design is if there is any coupled interaction between the atmosphere and the ocean. There is known coupling between atmospheric and oceanic variability in this region arising between the AMOC and the NAO (Delworth and Zeng 2016), which indicates that feedbacks could also be important for the NAWH. Future work that examines how changes in atmospheric

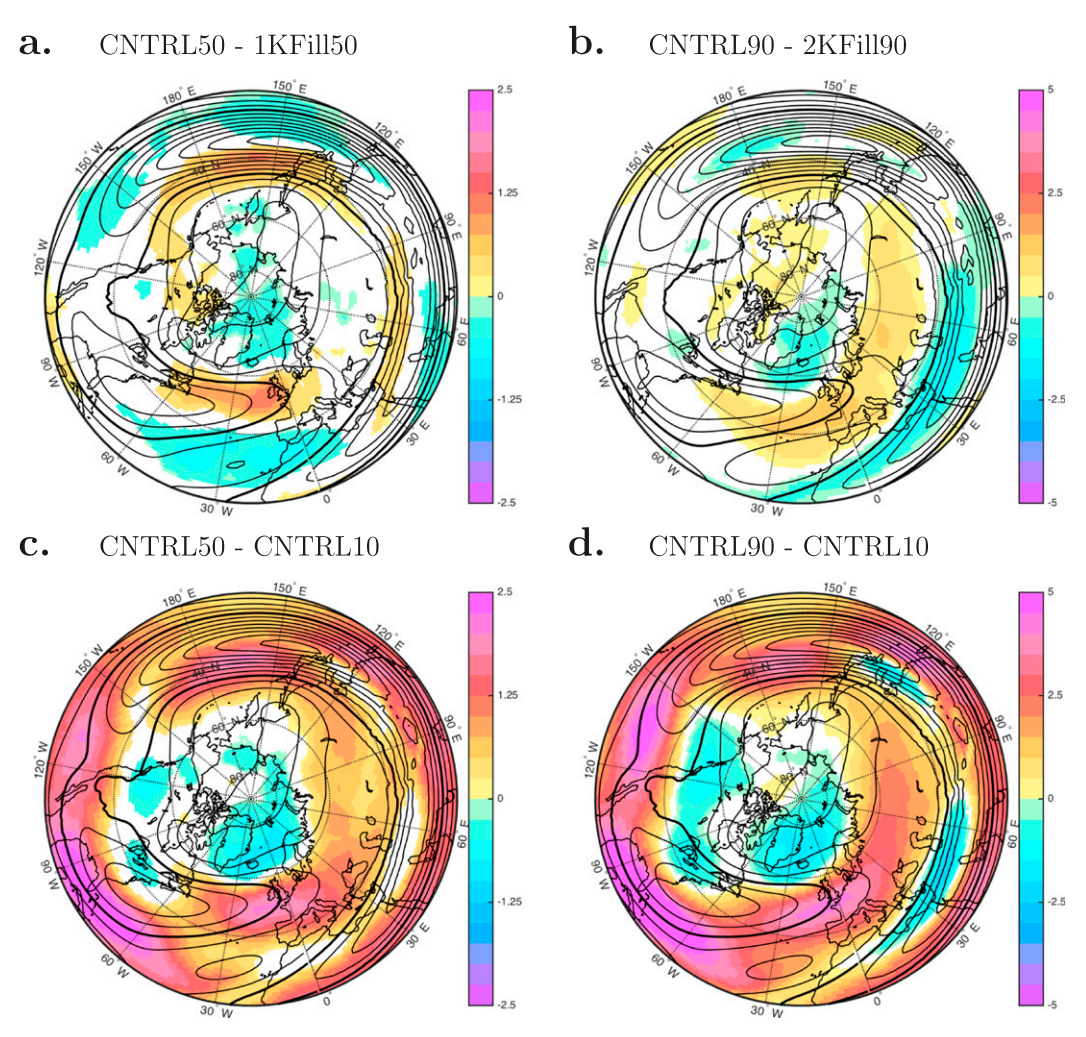


FIG. 8. December–February seasonal ensemble mean differences in wind speed on the dynamic tropopause (m s $^{-1}$) between (a) CNTRL50 and 1KFill50, (b) CNTRL90 and 2KFill90, (c) CNTRL50 and CNTRL10, and (d) CTNRL90 and CNTRL10. Only significant values at the 5% significance level as computed using a two-sided t test are shown. For reference, the 1KFill50, 2KFill90, CNTRL10, and CNTRL10 seasonal ensemble means in (a)–(d), respectively, are shown in black contours with the 30 m s $^{-1}$ contour in bold.

circulation induced by the NAWH might subsequently impact ocean circulation could provide further understanding of such feedbacks.

It is also important to highlight that missing processes within the model and model biases may have affected the present findings. For example, the more zonal configuration of the North Atlantic midlatitude jet compared to observations may introduce bias. Melting of the Greenland ice sheet is another important dynamic process that would be an important source of additional freshwater that could impact the strength of the warming hole (Gervais et al. 2018). If, for example, this additional melt led to a doubling of the depth of the warming hole the real climate response might be closer to the 2XDeep experiments.

Results from this study and previous work on midlatitude SST anomalies and their atmospheric impacts suggest that the response to the NAWH will be sensitive to the atmospheric base state and the NAWH's strength and location. In particular, it should be highlighted that an increased gradient in SST is likely of primary importance to the transient eddy forcing mechanism. This large dependence on the mean atmospheric state and SST gradient strength could also explain the discrepancies in previous work on this topic. Woollings et al. (2012) found a large response and produced their experimental SST change through freshwater hosing with SST anomalies spatially consistent with the control SST state. Prior studies that found a limited response to North Atlantic SST changes used methods in which the imposed SST anomalies were spatially inconsistent with the mean SST field. For example, as Harvey et al. (2015) states, their use of multimodel mean SST differences for their imposed SST anomalies smooths out the gradients in SST associated with the NAWH and may be partially responsible for the limited atmospheric response. Furthermore, the HadGAM1 model used in their study has a more tilted North Atlantic storm track than the multimodel mean, and thus the multimodel SST anomalies imposed may not be optimally located to impact the storm track in the HadGAM1. Ciasto et al. (2016) prescribed observed SSTs to force their atmospheric general circulation model simulations and imposed SST perturbations from fully coupled global climate model simulations. Because the observations have a different mean state than the fully coupled simulations, most notably with more tilted SST gradients, the imposed perturbations may not be coincident with the maximum gradients in the observed SSTs. Such studies that mix base states and SST anomalies from different sources may not produce an enhanced temperature gradient within the model's subpolar front, which is critical for generating the atmospheric response. If this is indeed the reason for the small responses in these studies, this has large implications for the methods that need to be employed to study this phenomenon.

Given the sensitivity of the atmospheric response to the details of NAWH formation and the atmospheric base state, the NAWH could be also be an important source of discrepancy between future climate projections in different models. Model differences in the development and strength of the warming hole are very likely (Menary and Wood 2018), although we do expect the location to be closely related to each model's mean oceanic structure. Given the large dependence of the response to the NAWH on the depth of the warming hole, differences in NAWH development could be an important factor in determining the location and magnitude of the response to the NAWH in future climate simulations and by extension the total climate change response. The mean state and climate change response of midlatitude and subtropical jets due to other changes in the system are also known to differ between climate simulations and they could be an important factor in the response to the NAWH in future climate projections.

Our results demonstrate that the NAWH significantly affects the North Atlantic jet in future simulations of the CESM. These findings improve understanding of how the development of the NAWH might influence atmospheric circulation within the CESM-LE and the true climate system more broadly. However, further work that examines the development and impact of the NAWH in different global climate models is needed to help further

understanding of these processes within global climate model projections and how a future warming hole might influence the atmosphere in the real world.

Acknowledgments. We would like to thank two anonymous reviewers and Sir Brian Hoskins for their helpful comments on the manuscript. This research was supported by NSF Grant AGS-1303542. Y. Kushnir's contribution to this study was funded by DOE Grant DE-SC0014423. This paper is LDEO Publication Number 8281. The CESM project is supported by the National Science Foundation and the Office of Science (BER) of the U.S. Department of Energy. This research was enabled by CISL compute and storage resources. Bluefire, a 4064-processor IBM Power6 resource with a peak of 77 TeraFLOPS, provided more than 7.5 million computing hours, the GLADE high-speed disk resources provided 0.4 PB (petabytes) of dedicated disk, and CISL's 12-PB HPSS archive provided over 1 PB of storage in support of this research project. Some computations for this research were performed on the Pennsylvania State University's Institute for Cyber-Science Advanced CyberInfrastructure (ICS-ACI). This content is solely the responsibility of the authors and does not necessarily represent the views of the Institute for CyberScience.

REFERENCES

Baker, H., T. Woollings, and C. Mbengue, 2017: Eddy-driven jet sensitivity to diabatic heating in an idealized GCM. *J. Climate*, 30, 6413–6431, https://doi.org/10.1175/JCLI-D-16-0864.1.

Barnes, E. A., and L. Polvani, 2013: Response of the midlatitude jets, and of their variability, to increased greenhouse gases in the CMIP5 models. *J. Climate*, 26, 7117–7135, https://doi.org/ 10.1175/JCLI-D-12-00536.1.

Böning, C. W., E. Behrens, A. Biastoch, and K. Getzla, 2016: Emerging impact of Greenland meltwater on deepwater formation in the North Atlantic Ocean. *Nat. Geosci.*, 9, 523–528, https://doi.org/10.1038/ngeo2740.

Brayshaw, D. J., B. Hoskins, and M. Blackburn, 2008: The storm-track response to idealized SST perturbations in an aquaplanet GCM. *J. Atmos. Sci.*, **65**, 2842–2860, https://doi.org/10.1175/2008JAS2657.1.

—, and —, 2011: The basic ingredients of the North Atlantic storm track. Part II: Sea surface temperatures. *J. Atmos. Sci.*, **68**, 1784–1805, https://doi.org/10.1175/2011JAS3674.1.

Chang, E. K. M., Y. Guo, and X. Xia, 2012: CMIP5 multimodel ensemble projection of storm track change under global warming. J. Geophys. Res., 117, D23118, https://doi.org/ 10.1029/2012JD018578.

Ciasto, L., C. Li, J. Wettstein, and N. Kvamsto, 2016: North Atlantic storm-track sensitivity to projected sea surface temperature: Local versus remote influences. J. Climate, 29, 6973– 6991, https://doi.org/10.1175/JCLI-D-15-0860.1.

Delworth, T. L., and F. Zeng, 2016: The impact of the North Atlantic Oscillation on climate through its influence on the

- Atlantic meridional overturning circulation. *J. Climate*, **29**, 941–962, https://doi.org/10.1175/JCLI-D-15-0396.1.
- Deser, C., G. Magnusdottir, R. Saravanan, and A. Phillips, 2004: The effects of North Atlantic SST and sea ice anomalies on the winter circulation in CCM3. Part II: Direct and indirect components of the response. *J. Climate*, 17, 877–889, https://doi.org/ 10.1175/1520-0442(2004)017<0877:TEONAS>2.0.CO;2.
- Drijfhout, S., G. J. van Oldenborgh, and A. Cimatoribus, 2012: Is a decline of AMOC causing the warming hole above the North Atlantic in observed and modeled warming patterns? *J. Climate*, 25, 8373–8379, https://doi.org/10.1175/JCLI-D-12-00490.1.
- Gervais, M., E. Atallah, J. R. Gyakum, and L. B. Tremblay, 2016: Arctic air masses in a warming world. *J. Climate*, **29**, 2359–2373, https://doi.org/10.1175/JCLI-D-15-0499.1.
- —, J. Shaman, and Y. Kushnir, 2018: Mechanisms governing the development of the North Atlantic warming hole in the CESM-LE future climate simulations. *J. Climate*, 31, 5927– 5946, https://doi.org/10.1175/JCLI-D-17-0635.1.
- Ghosh, R., W. A. Müller, J. Baehr, and J. Bader, 2017: Impact of observed North Atlantic multidecadal variations to European summer climate: A linear baroclinic response to surface heating. Climate Dyn., 48, 3547–3563, https://doi.org/10.1007/ s00382-016-3283-4.
- Haarsma, R. J., F. M. Selten, and S. S. Drijfhout, 2015: Decelerating Atlantic meridional overturning circulation main cause of future west European summer atmospheric circulation changes. *Environ. Res. Lett.*, 10, 094007, https://doi.org/10.1088/1748-9326/10/9/094007.
- Hall, N. M., H. Lin, and J. Derome, 2001: The extratropical signal generated by a midlatitude SST anomaly. Part II: Influence on seasonal forecasts. J. Climate, 14, 2696–2709, https://doi.org/ 10.1175/1520-0442(2001)014<2696:TESGBA>2.0.CO;2.
- Harvey, B. J., L. C. Shaffrey, T. J. Woollings, G. Zappa, and K. I. Hodges, 2012: How large are projected 21st century storm track changes? *Geophys. Res. Lett.*, 39, L18707, https://doi.org/ 10.1029/2012GL052873.
- —, and —, 2014: Equator-to-pole temperature differences and the extra-tropical storm track responses of the CMIP5 climate models. *Climate Dyn.*, 43, 1171–1182, https://doi.org/10.1007/s00382-013-1883-9.
- —, —, and —, 2015: Deconstructing the climate change response of the Northern Hemisphere wintertime storm tracks. *Climate Dyn.*, **45**, 2847–2860, https://doi.org/10.1007/s00382-015-2510-8.
- Held, I., 1983: Stationary and quasi-stationary eddies in the extratropical atmosphere: Theory. Large-Scale Dynamical Processes in the Atmosphere, B. Hoskins and R. Pearce, Eds., Academic Press, 127–168.
- Hendon, H. H., and D. L. Hartmann, 1982: Stationary waves on a sphere: Sensitivity to thermal feedback. *J. Atmos. Sci.*, 39, 1906–1920, https://doi.org/10.1175/1520-0469(1982)039<1906: SWOASS>2.0.CO;2.
- Hoskins, B. J., and D. J. Karoly, 1981: The steady linear response of a spherical atmosphere to thermal and orographic forcing. *J. Atmos. Sci.*, 38, 1179–1196, https://doi.org/10.1175/1520-0469(1981)038<1179:TSLROA>2.0.CO;2.
- ——, and T. Ambrizzi, 1993: Rossby wave propagation on a realistic longitudinally varying flow. J. Atmos. Sci., 50, 1661–1671, https:// doi.org/10.1175/1520-0469(1993)050<1661:RWPOAR>2.0.CO;2.
- —, I. James, and G. White, 1983: The shape, propagation and mean-flow interaction of large-scale weather systems. J. Atmos. Sci., 40, 1595–1612, https://doi.org/10.1175/1520-0469(1983)040<1595:TSPAMF>2.0.CO;2.

- Hurrell, J. W., and Coauthors, 2013: The Community Earth System Model: A framework for collaborative research. *Bull. Amer. Meteor. Soc.*, 94, 1339–1360, https://doi.org/10.1175/BAMS-D-12-00121.1.
- Inatsu, M., H. Mukougawa, and S.-P. Xie, 2003: Atmospheric response to zonal variations in midlatitude SST: Transient and stationary eddies and their feedback. *J. Climate*, 16, 3314–3329, https://doi.org/10.1175/1520-0442(2003)016<3314: ARTZVI>2.0.CO:2.
- Jahn, A., and M. M. Holland, 2013: Implications of Arctic sea ice changes for North Atlantic deep convection and the meridional overturning circulation in CCSM4-CMIP5 simulations. *Geophys. Res. Lett.*, 40, 1206–1211, https://doi.org/10.1002/ grl.50183.
- Kay, J. E., and Coauthors, 2015: The Community Earth System Model (CESM) large ensemble project: A community resource for studying climate change in the presence of internal climate variability. *Bull. Amer. Meteor. Soc.*, 96, 1333–1349, https://doi.org/10.1175/BAMS-D-13-00255.1.
- Kushnir, Y., W. A. Robinson, I. Bladé, N. M. J. Hall, S. Peng, and R. Sutton, 2002: Atmospheric GCM response to extratropical SST anomalies: Synthesis and evaluation. *J. Climate*, 15, 2233– 2256, https://doi.org/10.1175/1520-0442(2002)015<2233: AGRTES>2.0.CO;2.
- Lee, S., and H.-K. Kim, 2003: The dynamical relationship between subtropical and eddy-driven jets. *J. Atmos. Sci.*, **60**, 1490–1503, https://doi.org/10.1175/1520-0469(2003)060<1490: TDRBSA>2.0.CO;2.
- Magnusdottir, G., C. Deser, and R. Saravanan, 2004: The effects of North Atlantic SST and sea ice anomalies on the winter circulation in CCM3. Part I: Main features and storm track characteristics of the response. *J. Climate*, **17**, 857–876, https://doi.org/10.1175/1520-0442(2004)017<0857:TEONAS>2.0.
- Marshall, J., J. R. Scott, K. C. Armour, J. M. Campin, M. Kelley, and A. Romanou, 2015: The ocean's role in the transient response of climate to abrupt greenhouse gas forcing. *Climate Dyn.*, **44**, 2287–2299, https://doi.org/10.1007/s00382-014-2308-0.
- Menary, M. B., and R. A. Wood, 2018: An anatomy of the projected North Atlantic warming hole in CMIP5 models. Climate Dyn., 50, 3063–3080, https://doi.org/10.1007/s00382-017-3793-8.
- Nakamura, H., T. Sampe, Y. Tanimoto, and A. Shimpo, 2004: Observed associations among storm tracks, jet streams and midlatitude oceanic fronts. *Earth's Climate: The Ocean–Atmosphere Interaction*, Geophys. Monogr., Vol. 147, Amer. Geophys. Union, 329–345.
- Palmer, T. N., and Z. Sun, 1985: A modelling and observational study of the relationship between sea surface temperature in the North-West Atlantic and the atmospheric general circulation. *Quart. J. Roy. Meteor. Soc.*, 111, 947–975, https://doi. org/10.1002/qj.49711147003.
- Peng, S., and J. S. Whitaker, 1999: Mechanisms determining the atmospheric response to midlatitude SST anomalies. *J. Climate*, **12**, 1393–1408, https://doi.org/10.1175/1520-0442 (1999)012<1393:MDTART>2.0.CO;2.
- —, and W. A. Robinson, 2001: Relationships between atmospheric internal variability and the responses to an extratropical SST anomaly. *J. Climate*, 14, 2943–2959, https://doi.org/10.1175/1520-0442(2001)014<2943:RBAIVA>2.0.CO;2.
- Rahmstorf, S., J. E. Box, G. Feulner, M. E. Mann, A. Robinson, S. Rutherford, and E. J. Schaffernicht, 2015: Exceptional twentieth-century slowdown in Atlantic Ocean overturning

- circulation. *Nat. Climate Change*, **5**, 475–480, https://doi.org/10.1038/nclimate2554.
- Sévellec, F., A. V. Fedorov, and W. Liu, 2017: Arctic seaice decline weakens the Atlantic meridional overturning circulation. *Nat. Climate Change*, 7, 604–610, https://doi.org/ 10.1038/nclimate3353.
- Shaw, T. A., and Coauthors, 2016: Storm track processes and the opposing influences of climate change. *Nat. Geosci.*, 9, 656– 664, https://doi.org/10.1038/ngeo2783.
- Smeed, D. A., and Coauthors, 2014: Observed decline of the Atlantic meridional overturning circulation 2004–2012. *Ocean Sci.*, 10, 29–38, https://doi.org/10.5194/os-10-29-2014.
- —, and Coauthors, 2018: The North Atlantic Ocean is in a state of reduced overturning. *Geophys. Res. Lett.*, 45, 1527–1533, https://doi.org/10.1002/2017GL076350.
- Ting, M., and S. Peng, 1995: Dynamics of the early and middle winter atmospheric responses to the northwest Atlantic SST

- anomalies. *J. Climate*, **8**, 2239–2254, https://doi.org/10.1175/1520-0442(1995)008<2239:DOTEAM>2.0.CO:2.
- Wilson, C., B. Sinha, and R. G. Williams, 2009: The effect of ocean dynamics and orography on atmospheric storm tracks. *J. Climate*, 22, 3689–3702, https://doi.org/10.1175/2009JCLI2651.1.
- Winton, M., S. M. Griffies, B. L. Samuels, J. L. Sarmiento, and T. L. Frölicher, 2013: Connecting changing ocean circulation with changing climate. *J. Climate*, 26, 2268–2278, https://doi.org/10.1175/JCLI-D-12-00296.1.
- Woollings, T., and M. Blackburn, 2012: The North Atlantic jet stream under climate change and its relation to the NAO and EA patterns. *J. Climate*, **25**, 886–902, https://doi.org/10.1175/JCLI-D-11-00087.1.
- —, J. Gregory, J. Pinto, M. Reyers, and D. Brayshaw, 2012: Response of the North Atlantic storm track to climate change shaped by ocean–atmosphere coupling. *Nat. Geosci.*, **5**, 313–317, https://doi.org/10.1038/ngeo1438.